ANTIOXIDANTS & REDOX SIGNALING
Volume 16, Number 12, 2012

DOI: 10.1089/ars.2011.4175

ORIGINAL RESEARCH COMMUNICATION

Interleukin-13/-4-Induced Oxidative Stress Contributes to Death of Hippocampal Neurons in A$\beta_{1\text{-}42}$-Treated Hippocampus *In Vivo*

J.H. Nam,[1,2,*] K.W. Park,[1,2,*] E.S. Park,[1,2,*] Y.B. Lee,[3] H.G. Lee,[3] H.H. Baik,[1,2] Y.-S. Kim,[4] S. Maeng,[5] J. Park,[5] and B.K. Jin[1,2]

Abstract

Aims: The present study examined whether A$\beta_{1\text{-}42}$ can induce endogenous expression of interleukin-13 (IL-13) or (IL-4) within activated microglia in the rat hippocampus *in vivo.* We further investigated whether these cytokines mediate ROS/RNS generation through activation of NADPH oxidase and/or inducible nitric oxide synthase (iNOS), and thus contribute to the degeneration of hippocampal neurons *in vivo*. ***Results:*** Here, we show that IL-13 and IL-4, endogenously expressed in A$\beta_{1\text{-}42}$-activated microglia in hippocampus *in vivo*, contribute to degeneration of hippocampal neurons *in vivo*. Neutralization of IL-13 and IL-4 protected hippocampal neurons *in vivo* against neurotoxicity by inhibiting activation of microglial NADPH oxidase and iNOS, resulting in attenuation of ROS generation and oxidative damage of protein, lipid and DNA. ***Innovation:*** To our knowledge, this is the first study to demonstrate the possible involvement of endogenously expressed IL-13 and/or IL-4 in activated microglia after A$\beta_{1\text{-}42}$ injection in the degeneration of hippocampal neurons *in vivo*. The current findings suggest that the deleterious effects of microglia-derived endogenous IL-13 and/or IL-4 are involved in oxidative stress-mediated neurodegenerative diseases, such as AD. ***Conclusion:*** We carefully hypothesize that IL-13 and IL-4, well-known as anti-inflammatory cytokines might serve as neurotoxic mediators by enhancing microglia-derived oxidative stress in A$\beta_{1\text{-}42}$-treated hippocampus *in vivo. Antioxid. Redox Signal.* 16, 1369–1383.

Introduction

ALZHEIMER'S DISEASE (AD) is a chronic neurodegenerative disorder characterized by the presence of amyloid beta (Aβ) plaques and neurofibrillary tangles in brain areas associated with learning and memory functions. Deposition of Aβ, the main plaque component, is thought to play a critical role in the neuropathogenesis of AD (1, 48). Aβ plaques are surrounded by activated microglia in the area of AD pathology (17). In the rat hippocampus (38) and rat cortical cultures (30), Aβ has been shown to induce microglial activation.

Accumulating evidence has demonstrated that activated microglia produce reactive oxygen species (ROS), such as superoxide ($O_2\bullet^-$) and $O_2\bullet^-$-derived oxidants, which induce or exacerbate neurotoxicity by triggering oxidative stress in hippocampal (11) and cortical neurons (52), as well as dopaminergic neurons (13). Microglia-derived NADPH oxidase

Innovation

In general, IL-13 and IL-4 function is beneficial as well-known anti-inflammatory cytokines. However, our study clearly shows that IL-13 and IL-4, exclusively expressed in microglia, contribute to cell death of hippocampal neurons in A$\beta_{1\text{-}42}$-treated hippocampus *in vivo.* These cytokines mediate ROS generation through microglia-derived NADPH oxidase and/or iNOS activation and thus contribute to the degeneration of hippocampal neurons *in vivo*. Our current data provide new insights into understanding of IL-13 and/or IL-4-induced oxidative stress from microglia and offer hope in halting initiation and/or progression of microglia-derived oxidative stress-mediated neurodegenerative diseases, such as AD.

[1]Department of Biochemistry and Molecular Biology, and [2]Neurodegeneration Control Research Center, School of Medicine, Kyung Hee University, Seoul, Korea.
[3]Neuroscience Graduate Program, School of Medicine, Ajou University, Suwon Korea.
[4]Burnett School of Biomedical Sciences, College of Medicine, University of Central Florida, Orlando, Florida.
[5]Department of East-West Medicine, Graduate School of East-West Medical Science, Kyung Hee University, Yongin, Korea.
*These authors contributed equally to this work.

induces ROS production in the A$\beta_{1\text{-}42}$-treated hippocampus *in vivo* (50). NADPH oxidase is a multi-subunit enzyme composed of cytosolic subunits ($p47^{phox}$, $p67^{phox}$, and Rac1) and plasma membrane subunits ($gp91^{phox}$ and $gp22^{phox}$) that catalyzes the generation of superoxide radicals from oxygen (15). Activated NADPH oxidase promotes the translocation of cytosolic proteins to the plasma membrane, where they assemble with membrane-associated proteins for activation. A$\beta_{1\text{-}42}$ activates the NAPDH oxidase complex in microglia (4), which in turn, generate ROS and consequent oxidative stress, thus contributing to neurodegeneration (30). Additionally, NADPH oxidase is activated in the brains of AD patients, resulting in the formation of ROS (39). Several studies have demonstrated evidence of oxidative stress in the brains of AD patients, including oxidative modifications of proteins, lipids (19, 51), and DNA (25). These findings suggest that NADPH oxidase-mediated oxidative stress contributes to neurodegeneration in AD.

Earlier reports showed that interleukin-13 (IL-13) and interlukin-4 (IL-4), well-known anti-inflammatory cytokines, suppress the production of inflammatory mediators, such as tumor necrosis factor-α (TNF-α), interleukin-1β (IL-1β), and macrophage chemoattractant protein (MCP-1), from activated microglia *in vivo* and *in vitro* (8, 9, 43). These results were obtained after the exogenous application of IL-13 or IL-4, owing to no evidence of endogenous IL-13 or IL-4 in microglia. In contrast, recent studies by our group disclosed endogenous IL-13 or IL-4 expression in activated microglia of lipopolysaccharide (LPS)-treated rat cerebral cortices (36, 40) and thrombin-treated hippocampus (33, 34) *in vivo*.

Whereas beneficial effects of IL-13 or IL-4 have been reported, such as increased survival of mice in an experimental model of sepsis (27), multiple sclerosis (MS) (16), and ischemic conditions (55), harmful effects are also evident. For instance, in a mouse asthma model, allergic airway inflammation is inhibited upon treatment with an anti-IL-13 or IL-4 monoclonal antibody (5, 14, 45, 49, 53, 54). Additionally, in endothelial cells, IL-13 and IL-4 induce ROS production via activation of NADPH oxidase (18, 47). Recent studies by our group further showed that in thrombin-treated hippocampus, microglia-derived IL-13 and IL-4 induce ROS generation through activation of NADPH oxidase, leading to the degeneration of hippocampal neurons *in vivo* (33, 34).

In the present study, we examined whether A$\beta_{1\text{-}42}$ can induce endogenous expression of IL-13 or IL-4 within activated microglia in the rat hippocampus *in vivo.* We further investigated whether these cytokines mediate ROS generation through NADPH oxidase activation and thus contribute to the degeneration of hippocampal neurons *in vivo*.

Results

A$\beta_{1\text{-}42}$ induces neuronal death and microglial activation in the hippocampus in vivo

A$\beta_{1\text{-}42}$ (1 nmol) and A$\beta_{42\text{-}1}$ (1 nmol) as a control were unilaterally injected into the CA1 layer of the rat hippocampus. Seven days later, brains were removed and coronal sections were processed for immunostaining with an antibody against a neuronal nuclear protein (NeuN) and Nissl staining. In the A$\beta_{1\text{-}42}$-treated CA1 layer of hippocampus, there was a significant loss of NeuN-immunopositive (NeuN-ip) neurons (Fig. 1E), compared with intact (Fig. 1A) or A$\beta_{42\text{-}1}$-treated CA1 layer of the hippocampus (Fig. 1C). A$\beta_{1\text{-}42}$-induced neuronal death was further confirmed by staining for Nissl substance using sections adjacent to those used for NeuN immunostaining. Consistent with the results of NeuN immunostaining, there was a dramatic reduction of Nissl-stained cells in the CA1 area of the hippocampus in A$\beta_{1\text{-}42}$-treated animals (Fig. 1F), compared with intact (Fig. 1B) or A$\beta_{42\text{-}1}$-treated CA1 layer of the hippocampus (Fig. 1D).

We next examined the activation of microglia in the CA1 hippocampal area after A$\beta_{1\text{-}42}$ injection *in vivo*. Rat brain sections adjacent to those used for NeuN immunostaining in Figure 1 were processed for immunohistochemical staining with OX-42 (CD11b) and OX-6 (CD74) antibodies, which recognize complement receptor III and major histocompatibility complex II. In intact (Fig. 2A, a) or A$\beta_{42\text{-}1}$ (Fig. 2C, c)-injected CA1 layer of the hippocampus, OX-42-ip microglia exhibited the typical ramified morphology of resting microglia. By contrast, in the A$\beta_{1\text{-}42}$-injected hippocampus, the majority of OX-42-ip microglia displayed an activated morphology, including larger cell bodies with short, thick, or no processes (Fig. 2E, e). Similar patterns were observed for OX-6 immunohistochemical staining, which was performed on the sections adjacent to those used for OX-42 immunostaining. These results showed that, compared to intact (Fig. 2B, b) or A$\beta_{42\text{-}1}$ (Fig. 2D, d)-injected CA1 layer, A$\beta_{1\text{-}42}$ caused the appearance of many OX-6-ip cells in the CA1 layer of the hippocampus (Fig. 2F, f), in which hippocampal neurons were degenerated (Fig. 1)

Aβ$_{1\text{-}42}$ induces endogenous expression of IL-13 or IL-4 in the hippocampus in vivo

We investigated whether A$\beta_{1\text{-}42}$ could induce IL-13 or IL-4 protein expression in the hippocampal CA1 layer. Immunohistochemical analysis showed the expression of IL-13 (Figs. 3A–3D) or IL-4 (Figs. 3E–3H) as early as 24 h after A$\beta_{1\text{-}42}$ injection, which was maintained up 14 days, in hippocampal CA1 layer. The levels of IL-13 or IL-4 expression were measured after A$\beta_{1\text{-}42}$ injection using sandwich ELISA (Fig. 3I) and Western blotting (Fig. 3J). Similar to immunohistochemical data, IL-13 or IL-4 levels in the hippocampus were significantly increased as early as 24 h after A$\beta_{1\text{-}42}$ injection, and gradually increased up to 7 days after A$\beta_{1\text{-}42}$ injection.

IL-13 or IL-4 expression is localized within activated microglia in the Aβ$_{1\text{-}42}$-treated hippocampus in vivo *and APP/PS1 Tg-mouse*

To identify the cell types expressing IL-13 or IL-4 in the hippocampal CA1 layer, double-immuno fluorescence staining with antibodies against OX-42 (Figs. 4A, 4D, 4G) for microglia and IL-13 (Figs. 4B and 4E) or IL-4 (Figs. 4B and 4H) was performed at 7 days after intrahippocampal injection of A$\beta_{42\text{-}1}$ as a control (Figs. 4A–4C) or A$\beta_{1\text{-}42}$ (Figs. 4D–4I). Fluorescence image from each channel were merged from the same double-labeled section (Figs. 4C, 4F, and 4I), respectively. IL-13 (Fig. 4F) and IL-4 (Fig. 4I) were localized in OX-42-ip cells, but not in NeuN-ip neurons nor in GFAP-ip astrocytes (data not shown), indicating that IL-13 or IL-4 expression was localized exclusively within activated microglia.

Transgenic mice carrying mutations in both amyloid precursor protein (APP) and the presenilin-1(PS-1) transgenes offer a good model to study the role of Aβ in AD pathology (22). This animal model was accompanied by marked production of Aβ peptides and microglia activation at age of

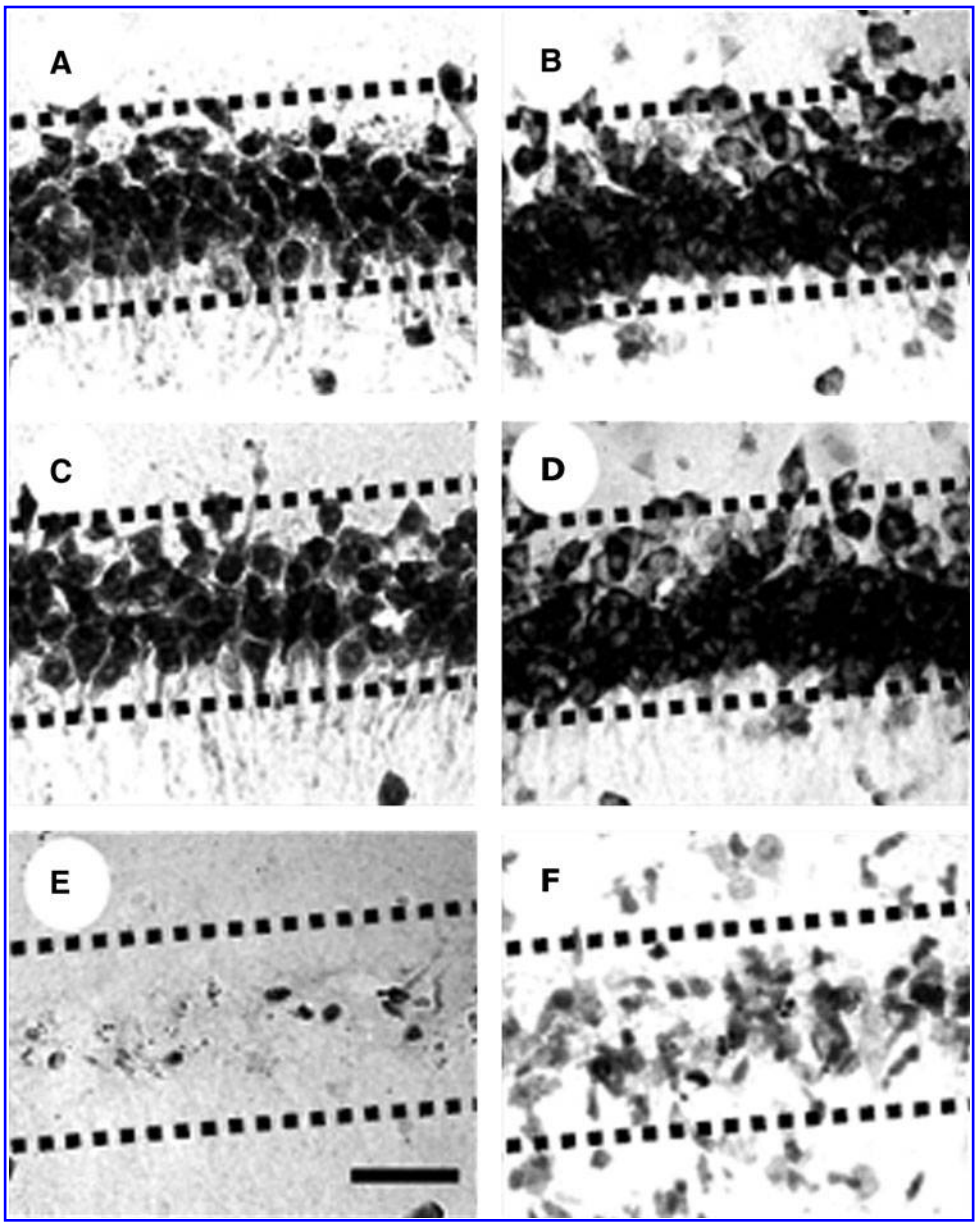

FIG. 1. Aβ$_{1-42}$-induced neurotoxicity in hippocampal CA1 region *in vivo*. Aβ_{42-1} (1 nmol) **(C, D)** as a control or Aβ_{1-42} (1 nmol) **(E, F)** was unilaterally injected into the CA1 layer of hippocampus. Seven days later, animals were sacrificed, brains were removed, and coronal sections were cut using a sliding microtome. Every sixth serial section was selected and processed for NeuN immunostaining **(A, C, E)** or Nissl staining **(B, D, F)**. Note a significant reduction of NeuN-immunopositive or Nissl-positive cells in Aβ_{1-42}-injected hippocampus, compared to intact **(A, B)** or Aβ_{42-1} injected tissue **(C, D)** as a control. These data are representative of 8–10 animals per group. *Dotted lines* indicate the CA1 layer of the hippocampus. Scale bar, 200 μm.

10 months (17). Thus, we determined the localization of IL-13 or IL-4 expression in APP/PS1 Tg-mouse. Brain sections from nontransgenic 10-month-age as controls (Figs. 4J–4L) or 10-month-age Tg-mouse (Figs. 4M–4R) were prepared for double-immunofluorescence staining with antibodies against MAC-1 (Figs. 4J, 4M, and 4P) for microglia and IL-13 (Figs. 4K and 4N) or MAC-1 and IL-4 (Figs. 4K and 4Q). Compared to control (Fig. 4L), IL-13 (Fig. 4O) or IL-4 (Fig. 4R) was expressed and localized within MAC-1-ip activated microglia. Additional experiment revealed that IL-13 or IL-4 expression in MAC-1-ip microglia was also detected in 12-month-age APP/PS1 Tg-mouse (data not shown).

IL-13 or IL-4 contributes to neurodegeneration in the hippocampus in vivo

We examined the role of IL-13 or IL-4 in Aβ_{1-42}-induced neuronal damage of hippocampus *in vivo* by administration of IL-13 neutralizing antibody (NA) or IL-4NA. At 7 days after intrahippocampal co-injection of Aβ_{1-42} with IL-13NA (Figs. 5E and 5F) or IL-4NA (Figs. 5G and 5H), NeuN immunocytochemical (A, C, E, G) and Nissl (B, D, F, H) staining revealed that IL-13NA or IL-4NA partially protected neurons from Aβ_{1-42} neurotoxicity (Figs. 5C and 5D). When expressed as the percentage of NeuN-ip cells on the ipsilateral versus the contralateral side, treatment with IL-13NA or IL-4NA increased the number of NeuN-ip neurons in the CA1 layer of the hippocampus about 33% and 24%, respectively (Fig. 5I), compared to those of Aβ_{1-42} only. As a control, nonspecific goat IgG with or without Aβ_{1-42} had little effect, similar to that observed with injection of Aβ_{1-42} only.

IL-13 or IL-4 contributes to the expression of iNOS in the hippocampus in vivo

It has been shown that Aβ_{1-42} induces microglia-derived iNOS expression in the hippocampus, contributing to neurodegeneration *in vivo* (28). Accordingly, we examined whether

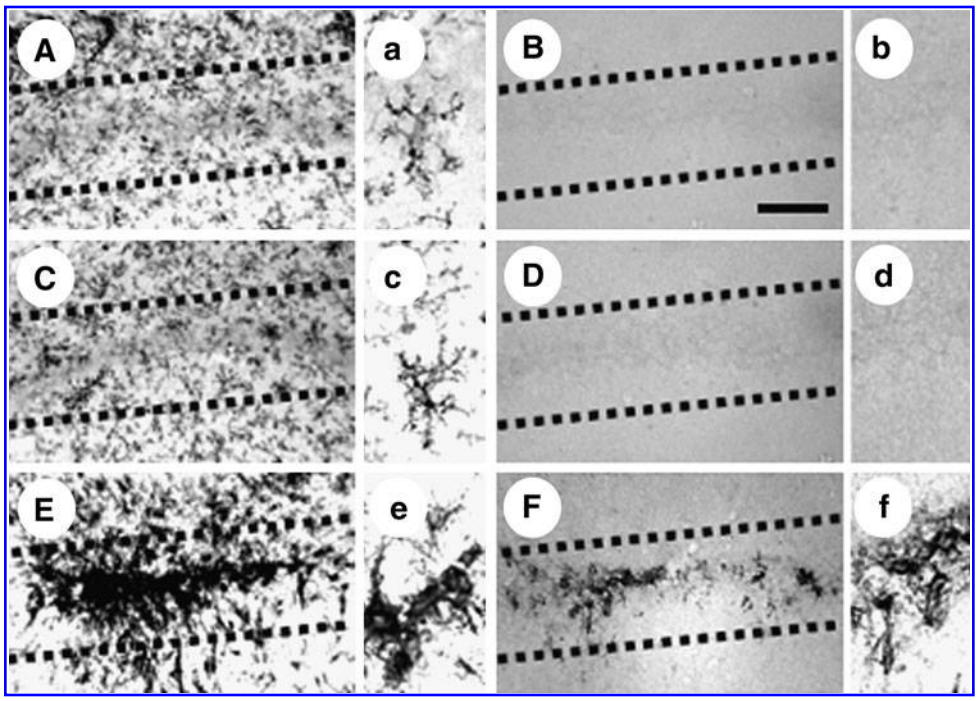

FIG. 2. $A\beta_{1-42}$-induced microglial activation in the CA1 layer of hippocampus. Sections (**A, B,** intact; **C, D,** $A\beta_{42-1}$; **E, F,** $A\beta_{1-42}$) adjacent to those used in Figure 1 were immunostained with OX-42 **(A, C, E)** or OX-6 **(B, D, F)** antibodies for microglia. The data are representative of 8–10 animals used for each experimental group. **(a–f)** Higher magnifications of **A–F**, respectively. *Dotted lines* indicate the CA1 layer of the hippocampus. Scale bar, 100 μm.

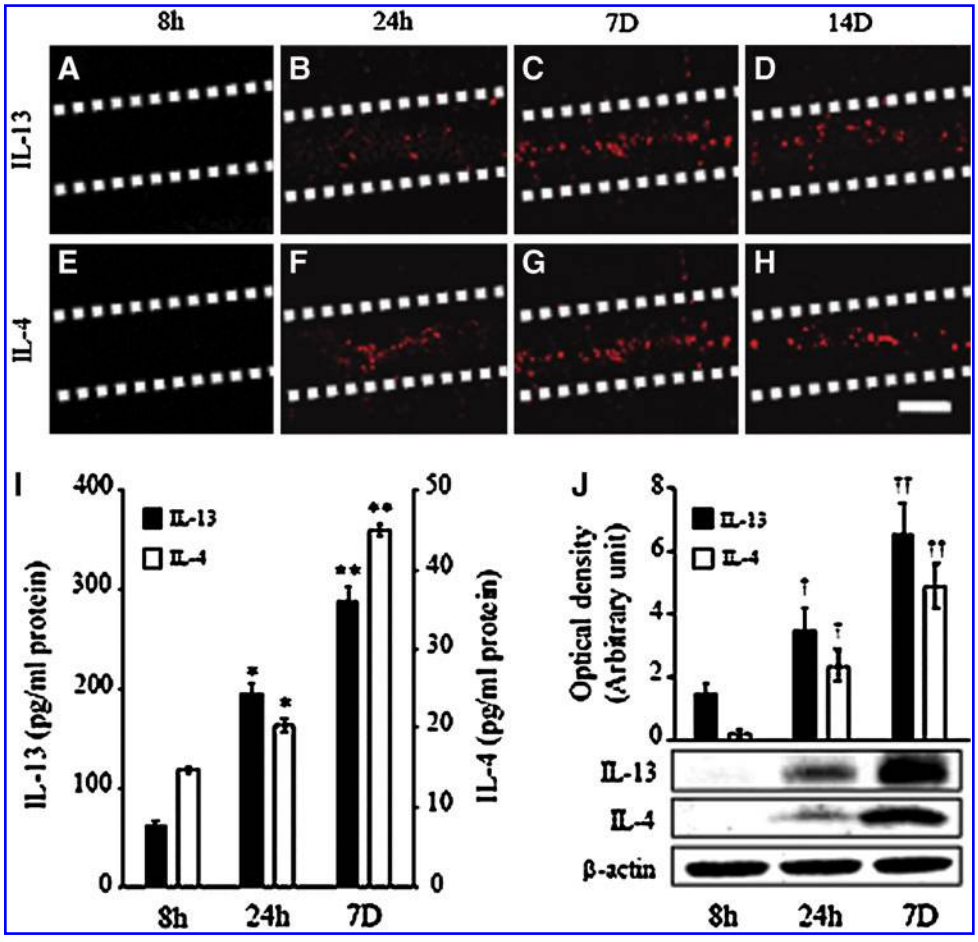

FIG. 3. IL-13 or IL-4 expression in the CA1 layer of hippocampus. $A\beta_{1-42}$ was injected into the hippocampal CA1 regions and animals were sacrificed at various time points. Brain sections were processed for immunostaining with IL-13 **(A–D)** or IL-4 antibody **(E–H)** at 8 h **(A, E)**, 24 h **(B, F)**, 7 days **(C, G)**, and 14 days **(D, H)** post-injection, respectively. Data are representative of 6–7 animals per group. *Dotted lines* indicate the CA1 layer of the hippocampus. Scale bar, 100 μm. **(I, J)** Kinetics of IL-13 or IL-4 levels in the hippocampus at the indicated time points after intrahippocampal injection of $A\beta_{1-42}$. The amounts of IL-13 or IL-4 were measured using sandwich ELISA technique **(I)** and Western blotting **(J).** Each bar represents the mean ± SEM of 5–6 animals per group; $^{*}p < 0.001$, $^{**}p < 0.001$, $^{\dagger}p < 0.05$, $^{\dagger\dagger}p < 0.001$ compared with 8 h injected control (ANOVA and Student-Newman-Keuls analyses).

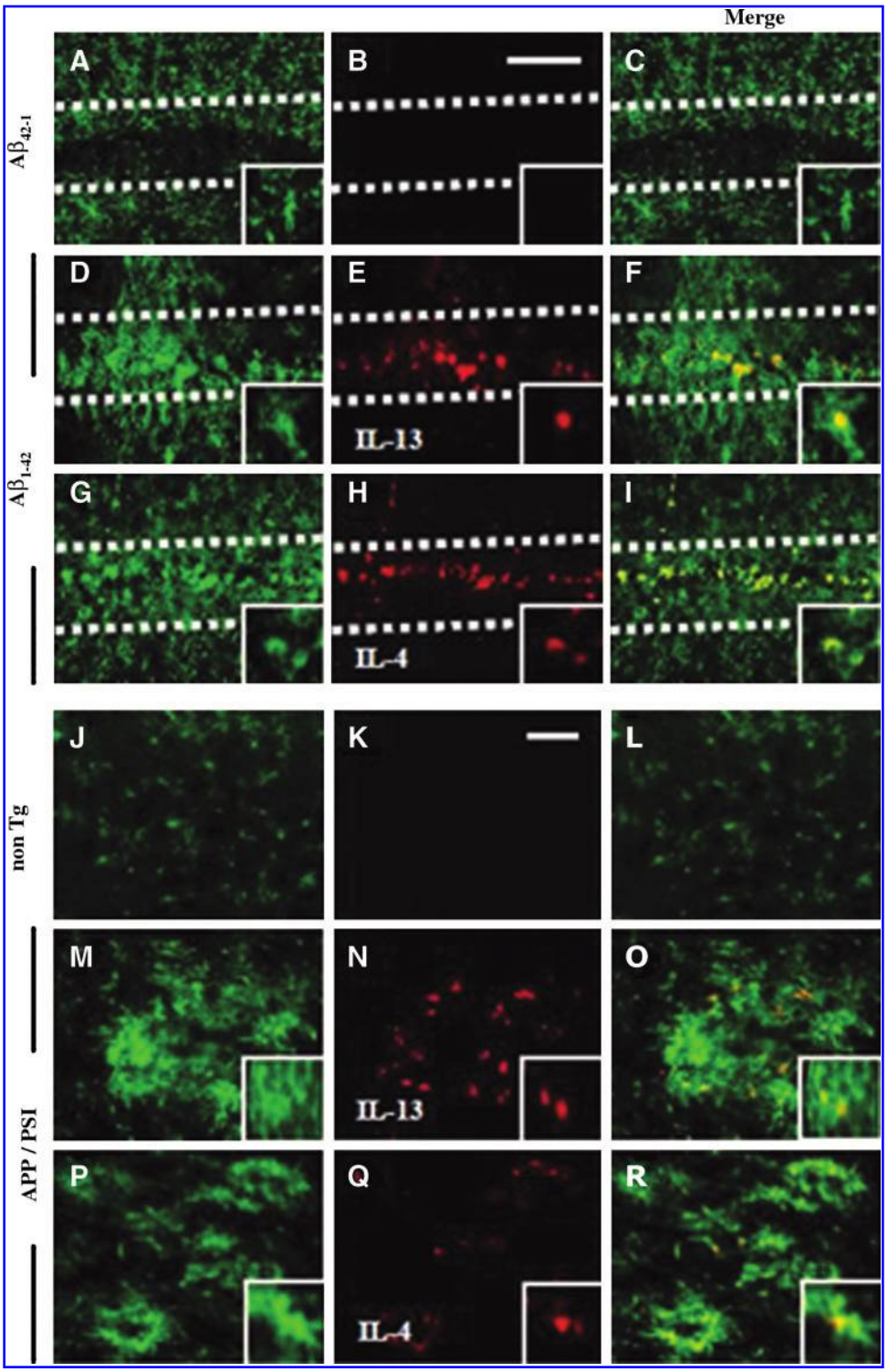

FIG. 4. Co-localization of IL-13 or IL-4 expression within the activated microglia in the CA1 layer of hippocampus and APP/PS1 Tg-mice. The sections were prepared 7 days after intrahippocampal injection of A$\beta_{42\text{-}1}$ as a control or A$\beta_{1\text{-}42}$ and then immunostained with OX-42 **(A, D, G)** for microglia and IL-13 antibody **(B, E)** or IL-4 antibody **(B, H).** Images from the same double-labeled tissue were merged **(C, F, I)**. Note the localization of IL-13 or IL-4 immunoreactivity within activated microglia. Scale bar, 100 μm. Co-localization of IL-13 or IL-4 expression within the activated microglia in APP/PS1 double transgenic mouse. Brains from nontransgenic control or 10-month-old APP/PS1 transgenic mouse were removed, and horizontal sections were cut using a sliding microtome. The sections were immunostained with MAC-1 **(J, M, P)** for microglia and IL-13 antibody **(K, N)** or IL-4 antibody **(K, Q).** Images from the same double-labeled tissue were merged **(L, O, R).** Note the localization of IL-13 or IL-4 immunoreactivity within activated microglia. Scale bar, 25 μm.

A$\beta_{1\text{-}42}$-induced expression of iNOS in the hippocampus might be affected by IL-13 or IL-4. Western blot analysis showed that A$\beta_{1\text{-}42}$ enhanced the expression of iNOS protein as early as 1 day after A$\beta_{1\text{-}42}$ treatment, with maximal levels attained 7 days after injection (Fig. 6A). Additional Western blot analysis disclosed that IL-13NA or IL-4NA significantly decreased iNOs protein levels by 39% and by 48%, respectively (Fig. 6B) at 3 days post-treatment.

IL-13 or IL-4 contributes to ROS production via *NADPH oxidase in the hippocampus* in vivo

Accumulating evidence shows A$\beta_{1\text{-}42}$ induces ROS generation through NADPH oxidase, and this resulted in neurodegeneration in rat hippocampus (4). We have recently shown that in thrombin-treated hipoocampus, microglia-derived IL-13 or IL-4 triggers ROS generation through

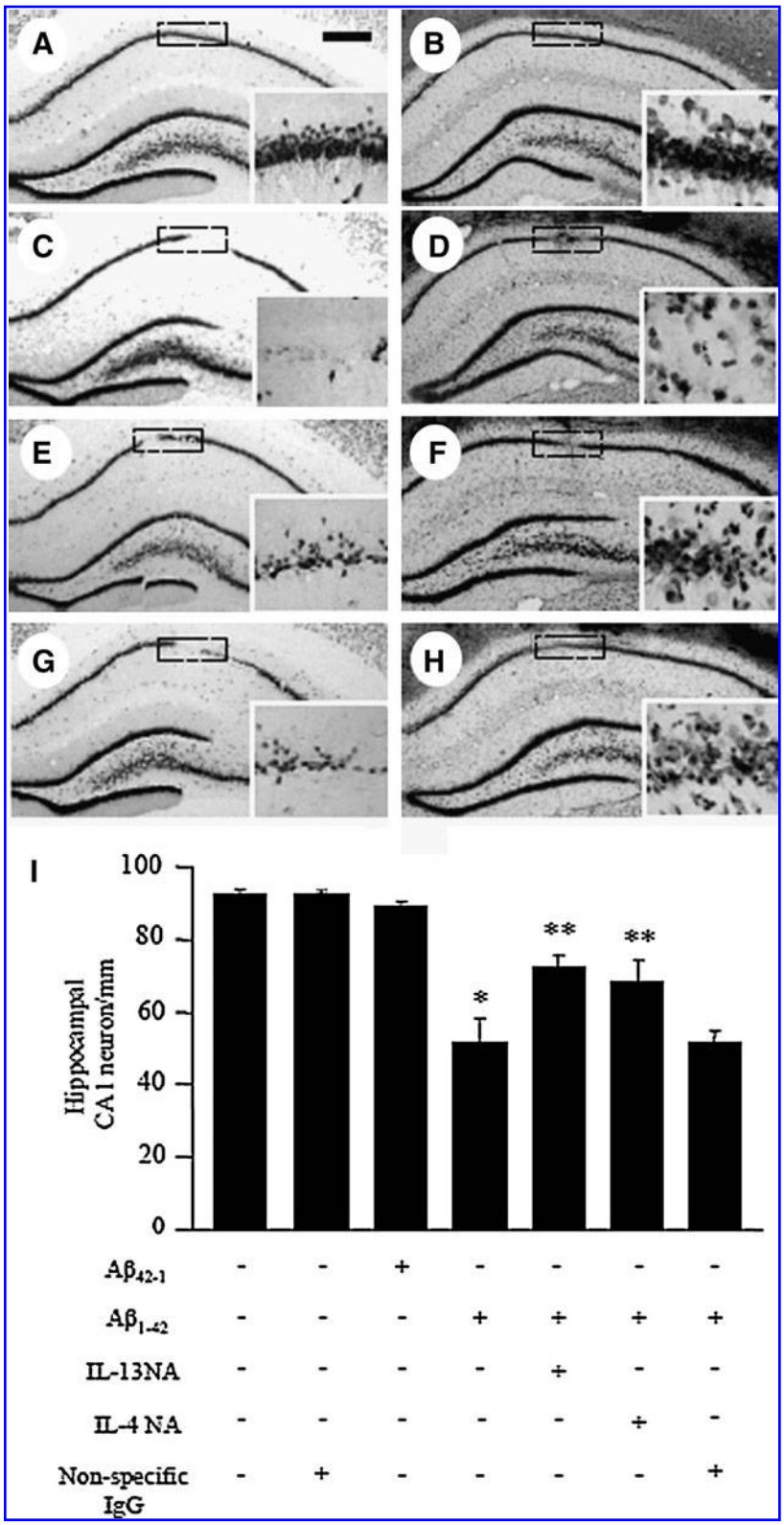

FIG. 5. IL-13 or IL-4 mediates $A\beta_{1-42}$-induced neuronal death in the hippocampus *in vivo*. $A\beta_{42-1}$ **(A, B)** as a control and $A\beta_{1-42}$ in the absence **(C, D)** or presence of IL-13NA antibody **(E, F)**, or IL-4 NA **(G, H)** was unilaterally injected into the hippocampus. Animals were sacrificed 7 days after injection. The brain sections were processed for NeuN immunostaining **(A, C, E, G)** and Nissl staining **(B, D, F, H)**. Scale bar, 500 μm. *Insets* show magnified photomicrographs of the area in the CA1 layer marked by *dotted rectangles*, respectively. Number of NeuN-immunopositive neurons in the CA1 layer of hippocampi treated with $A\beta_{1-42}$ in the absence or presence of IL-13 NA (1 μg/μl) or IL-4 NA (1 μg/μl). *Error bars* represent the means ± SEM from 6–7 samples per group **(I).** $^{*}p < 0.001$ compared with $A\beta_{42-1}$, $^{**}p < 0.01$ compared with hippocampi treated with $A\beta_{1-42}$ only (ANOVA and Student-Newman-Keuls analyses).

NADPH oxidase *in vivo*, resulting in neuronal cell death in thrombin-treated hipoocampus (33, 34). We hypothesized that $A\beta_{1-42}$-induced IL-13 or IL-4 takes part in ROS generation via NADPH oxidase in the hippocampus *in vivo* and resultant neurodegeneration. To test this possibility, hydroethidine histochemistry was performed to analyze *in situ* ROS production (11). The fluorescent products of oxidized hydroethidine (ethidium; red fluorescence) were increased significantly 5 days after injection (Fig. 7B), compared with $A\beta_{42-1}$-injected controls (Fig. 7A). In contrast, neutralization of IL-13 (Fig. 7C) or IL-4 (Fig. 7D) dramatically decreased $A\beta_{1-42}$-induced ethidium accumulation, indicative of IL-13

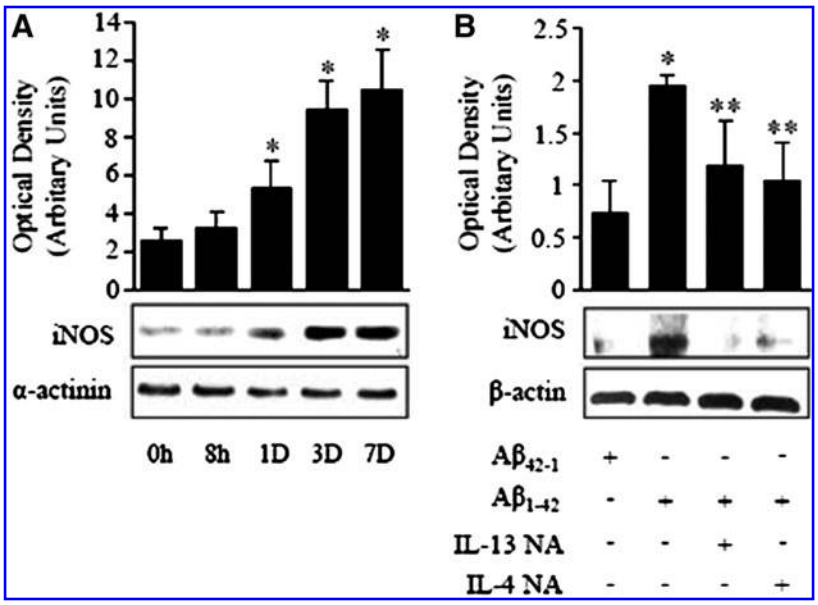

FIG. 6. IL-13 or IL-4 produces iNOS expression. Western blot analysis of iNOS expression in hippocampus at indicated time points after intrahippocampal $A\beta_{1\text{-}42}$ injection. The results represent the means ± SEM of three separate experiments **(A).** $^*p < 0.05$, compared with control 0 h (ANOVA and Student-Newman-Keuls analyses). Western blot analysis of iNOS expression at 3 days after intrahippocampal injection of $A\beta_{42\text{-}1}$, $A\beta_{1\text{-}42}$, $A\beta_{1\text{-}42}$ + IL-13 NA (1 μg/μl) or IL-4 NA (1 μg/μl). The results represent the means ± SEM of three separate experiments **(B)**. $^*p < 0.05$, compared with $A\beta_{42\text{-}1}$, $^{**}p < 0.05$, compared with $A\beta_{1\text{-}42}$ (ANOVA and Student-Newman-Keuls analyses).

or IL-4 involvement in ROS generation in the hippocampus *in vivo*.

Next, we investigated whether IL-13 or IL-4-induced ROS production was mediated by activation of microglial NADPH oxidase in the $A\beta_{1\text{-}42}$-treated hippocampus *in vivo*. To test this, we measured the translocation of $p47^{phox}$, $p67^{phox}$, and Rac-1, NADPH oxidase cytosolic subunits, from cytosol to plasma membrane in the hippocampus *in vivo*. Western blot analyses showed that, compared to $A\beta_{42\text{-}1}$-treated control, levels of cytosolic NADPH oxidase subunits ($p47^{phox}$, $p67^{phox}$, and Rac-1) were significantly increased in membrane components (Fig. 7E), indicating translocation and activation of NADPH oxidase complex in $A\beta_{1\text{-}42}$-treated hippocampus. Neutralization of IL-13 or IL-4 led to reduced levels of $p47^{phox}$, $p67^{phox}$, and Rac-1 in both the cytosolic and plasma membrane factions compared to $A\beta_{1\text{-}42}$-treated samples (Fig. 7E). This result indicates that IL-13 or IL-4 mediates translocation and activation of the NADPH oxidase complex. When quantified and expressed as ratio membrane fraction to total, injection of IL-13NA inhibited $p47^{phox}$ by 37%, $p67^{phox}$ by 18%, and Rac1 by 18%, and IL-4NA inhibited $p47^{phox}$ by 10%, $p67^{phox}$ by 26%, and Rac1 by 34% (Fig. 7F), respectively. Additional double-immunofluorescence staining showed that immunoreactivity to $p47^{phox}$ (Figs. 7G and 7I) and $p67^{phox}$ (Figs. 7H and 7J) was localized to activated microglia within the CA1 layer of the hippocampus 5 days after treatment with $A\beta_{1\text{-}42}$ (Figs. 7G and 7H) or 12-month-age APP/PS1 Tg-mouse (Figs. 7I and 7J). These immunoreactivities were undetectable in CA1 layer of hippocampus treated with $A\beta_{42\text{-}1}$ or of 12-month-age mice as controls (data not shown).

To examine the extent of the oxidative damage to proteins, we assessed protein carbonyl levels after $A\beta_{1\text{-}42}$ injection, with or without IL-13NA or IL-4NA into the hippocampus (33, 34). Carbonyl levels were measured by Western blotting, band intensities were compared (Fig. 8A). The increased levels of protein carbonyls in $A\beta_{1\text{-}42}$-injected samples were inhibited by 40% or by 31% at 5 days after intrahippocampal injection of IL-13NA or IL-4NA, respectively (Fig. 8B). IL-13NA or IL-4NA alone had no effects (data not shown). To investigate effects of IL-13 or IL-4 on $A\beta_{1\text{-}42}$-induced lipid peroxidation, we assessed MDA and HNE levels in hippocampal tissues after $A\beta_{1\text{-}42}$ injection with or without IL-13NA or IL-4NA into the hippocampus. Western blot analysis showed that MDA (Fig. 8C) and HNE (Fig. 8E) levels were significantly increased in the CA1 layer of hippocampus of $A\beta_{1\text{-}42}$-treated rat. $A\beta_{1\text{-}42}$-induced increase of MDA levels was significantly attenuated by 44% or by 28% at 5 days after intrahippocampal injection of IL-13NA or IL-4NA, respectively (Fig. 8D). Moreover, HNE Western levels were significantly decreased by 22% or by 25% at 5 days after intrahippocampal injection of IL-13NA or IL-4NA (Fig. 8F). IL-13NA or IL-4NA alone had no effects (data not shown). To assess the effects of IL-13 or IL-4 on $A\beta_{1\text{-}42}$-induced oxidative damage in nucleic acids, we performed immunostaining with an anti-8-OHdG antibody in the CA1 layer of hippocampus after $A\beta_{1\text{-}42}$ injection with or without IL-13NA or IL-4NA into the hippocampus. Consistent with observed changes in protein carbonyls and lipid oxidation (MDA and 4-HNE), there was substantial increase of 8-OHdG content in the CA1 layer of hippocampus 5 days after injection (Fig. 8G). This $A\beta_{1\text{-}42}$-induced increase in 8-OHdG levels was almost completely abrogated in the hippocampus of animals treated with IL-13NA or IL-4NA, respectively. Moreover, 8-OHdG levels using sandwich ELISA were significantly decreased by 34% or by 28% at 5 days after intrahippocampal injection of IL-13NA or IL-4NA, respectively (Fig. 8H). IL-13NA or IL-4NA alone had no effects (data not shown).

In the separate experiments, NeuN immunostaining demonstrated that the antioxidants, trolox (50 mg/kg, i.p.) or NAC (150 mg/kg, i.p.), protected hippocampal neurons from $A\beta_{1\text{-}42}$ neurotoxicity (Supplementary Fig. S1; supplementary data are available online at www.liebertonline.com/ars). These antioxidants also reduced the levels of the oxidative damage to proteins, lipid, and DNA (Supplementary Fig. 2), indicating that $A\beta_{1\text{-}42}$-increased ROS contributed to neurodegeneration of hippocampus *in vivo*.

Discussion

Aβ plaques represent a well-known histopathological feature of AD (1, 48), and consist of amyloid peptides, such as

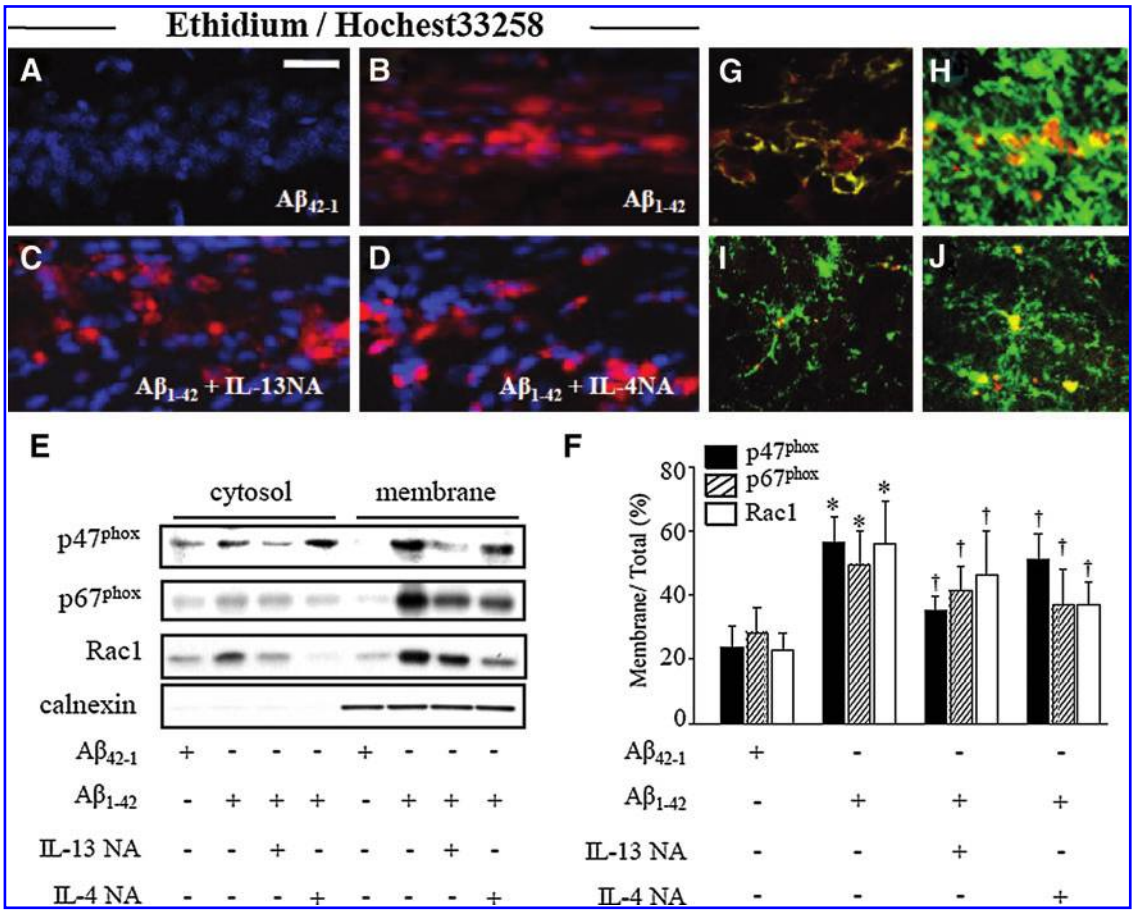

FIG. 7. IL-13 or IL-4 contributes to activation of NADPH oxidase and generation of reactive oxygen species (ROS). *In situ* visualization of superoxide ($O_2\bullet-$) and $O_2\bullet-$-derived oxidant production. Animals were injected with hydroethidine 5 days after intrahippocampal injection of A$\beta_{42\text{-}1}$ **(A)**, A$\beta_{1\text{-}42}$ in the absence **(B)**, or presence of IL-13 NA (1 μg/μl) **(C)**, or IL-4 NA (1 μg/μl) **(D)**. Confocal micrographs show ethidium fluorescence. Nuclei were counterstained with Hocheset33258. Scale bar: 50 μm. A$\beta_{1\text{-}42}$-induced activation of NADPH oxidase is inhibited by IL-13 NA or IL-4 NA. Tissue lysates from the ipsilateral hippocampus were prepared 3 days after intrahippocampal injection of A$\beta_{42\text{-}1}$ or A$\beta_{1\text{-}42}$ (1 nmol) in the absence or presence of IL-13 NA or IL-4 NA. Fractionated proteins were analyzed by SDS–PAGE and subjected to immunoblotting with anti-p47^{phox}, p67^{phox}, and Rac-1 antibody. The blots were reprobed with antibodies against the calnexin membrane protein as loading controls to exhibit fractionation efficiency **(E)**. The histogram shows quantitation of p47^{phox}, p67^{phox}, and Rac-1 levels expressed as the ratio of membrane fraction to total. The results represent the means ± SEM of 4–5 separate experiments **(F)**. *$p < 0.05$, compared with A$\beta_{42\text{-}1}$; †$p < 0.05$, compared with A$\beta_{1\text{-}42}$ only (ANOVA and Student-Newman-Keuls analyses). Localization of p47^{phox} and p67^{phox} immunoreactivity within activated microglia in A$\beta_{1\text{-}42}$-treated rat hippocampus or 10-month-age APP/PS1 Tg-mouse **(G–J)**. The sections of hippocampus were prepared 5 days after A$\beta_{1\text{-}42}$ injection into the rat hippocampus **(G, H)** or 10 month old APP/PS1 Tg-mouse **(I, J)** and stained with an antibody against p47^{phox} **(G, I),** or p67^{phox} **(H, J)**, and tomato lectin for microglia. Confocal images were captured from same area and merged **(G-J)**. Scale bar; 20 μm.

A$\beta_{1\text{-}42}$, A$\beta_{1\text{-}40}$, and A$\beta_{25\text{-}35}$ (29). These peptides are formed by the proteolytic cleavage of amyloid precursor protein (APP) by β-secretase and γ-secretase (44). A$\beta_{1\text{-}42}$ is increased to a more significant extent than other peptides in the human AD brain and AD transgenic mice (48), suggesting that the peptide is one of the major neuropathological factors in AD. Several studies have demonstrated the A$\beta_{1\text{-}42}$-triggered degeneration of hippocampal or cortical neurons and microglial activation *in vivo* (38) and *in vitro* (30, 42). These numerous findings of A$\beta_{1\text{-}42}$-induced neurotoxicity and microglial activation have been further confirmed by our current results showing that intrahippocampal injection of A$\beta_{1\text{-}42}$ induces substantial loss of hippocampal CA1 neurons and microglial activation *in vivo*.

IL-13 or IL-4, well-known anti-inflammatory cytokines, inhibit the production of inflammatory mediators, such as IL-6, IL-1β, MCP-1, TNF-α, and iNOS, possibly leading to increased cell survival (32, 43). In an experimental model of sepsis, endogenous IL-13 contributed to survival in mice by suppressing the excessive production of inflammatory cytokines and chemokines, including TNF-α and MIP-1α (27). Exogenous human recombinant IL-13 has been shown to inhibit the development of experimental autoimmune disease and expression of pro-inflammatory cytokines, such as TNF-α and IL-1β, in a demyelinating disease model of the CNS (8). Exogenous IL-4 contributes to increased MHC-II expression and decreased levels of inflammatory cytokines, such as TNF-α in LPS and A$\beta_{1\text{-}40}$-treated hippocampal slices co-cultured

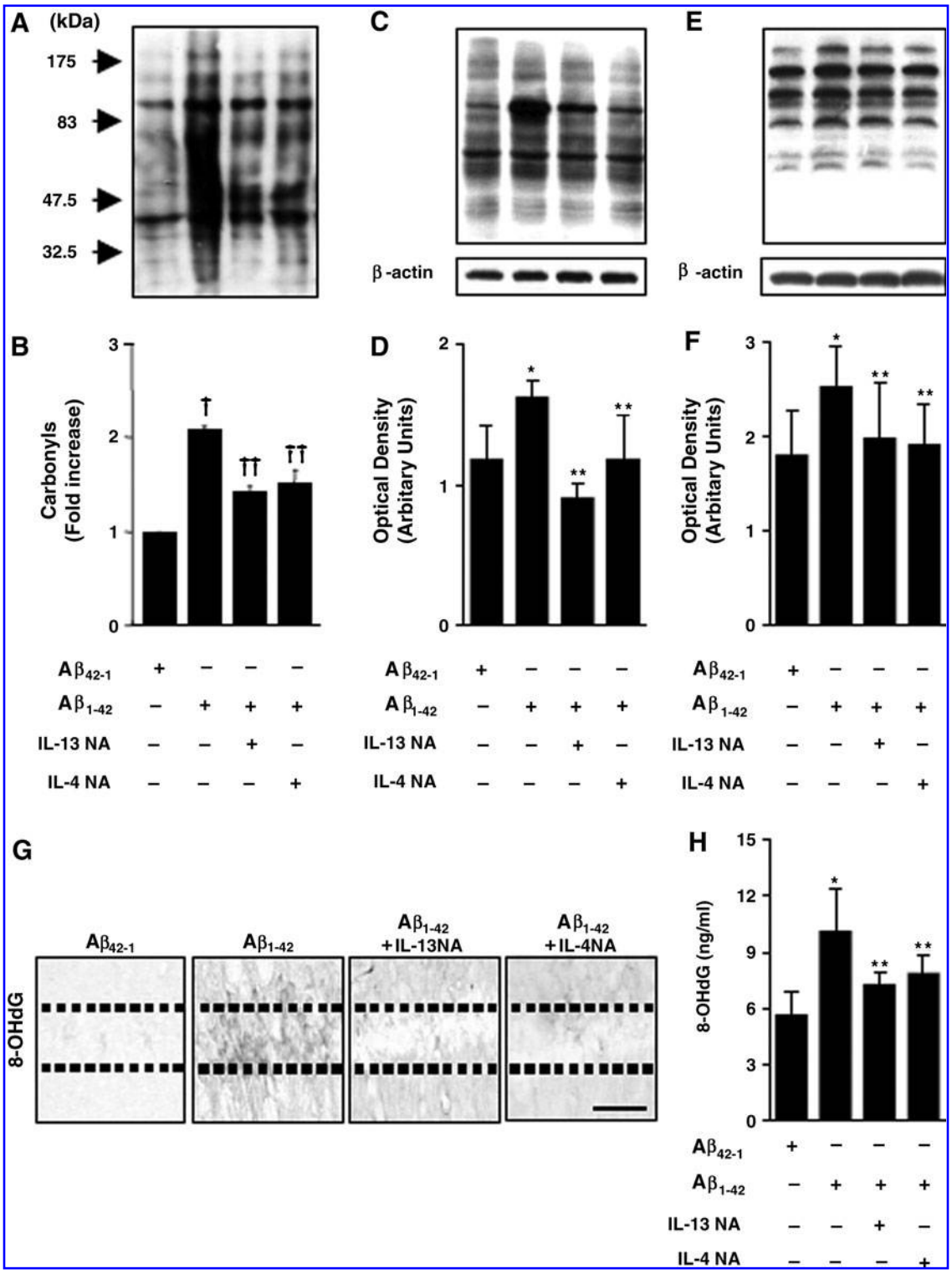

FIG. 8. IL-13 or IL-4 contributes to oxidative stress of protein, lipid, and DNA. Animals were decapitated 5 days after intrahippocampal injection of A$\beta_{42\text{-}1}$, A$\beta_{1\text{-}42}$, A$\beta_{1\text{-}42}$ + IL-13 NA (1 μg/μl), or IL-4 NA (1 μg/μl). Samples were analyzed by Western blotting for protein carbonyls as markers of oxidative modified proteins **(A)**. *Bars* represent the means ± SEM of four separate samples **(B)**. †$p < 0.001$, compared with A$\beta_{42\text{-}1}$; ††$p < 0.01$ compared with hippocampi treated with A$\beta_{1\text{-}42}$ only (ANOVA and Student-Newman-Keuls analyses). Samples were analyzed by Western blotting for MDA (malondialdehyde) as markers of lipid oxidation **(C)**. *Bars* represent the means ± SEM of four separate samples **(D)**. *$p < 0.05$, compared with A$\beta_{42\text{-}1}$; **$p < 0.05$ compared with hippocampi treated with A$\beta_{1\text{-}42}$ only (ANOVA and Student-Newman-Keuls analyses). Samples were analyzed by Western blotting for HNE (4-hydroxy-2-nonenal) as marker of lipid oxidation **(E)**. *Bars* represent the means ± SEM of four separate samples **(F)**. *$p < 0.05$, compared with A$\beta_{42\text{-}1}$; **$p < 0.05$ compared with hippocampi treated with A$\beta_{1\text{-}42}$ only (ANOVA and Student-Newman-Keuls analyses). The brain section was processed for 8-OHdG immunostaining. Scale bar, 35 μm **(G)**. The amounts of 8-OHdG were measured using sandwich ELISA technique **(H)**. *Bars* represent the means ± SEM of four separate samples. *$p < 0.01$, compared with A$\beta_{42\text{-}1}$; **$p < 0.05$ compared with hippocampi treated with A$\beta_{1\text{-}42}$ only (ANOVA and Student-Newman-Keuls analyses).

with cortical microglia, promoting the survival of hippocampal neurons (6). Moreover, exogenous IL-4 attenuates A$\beta_{1\text{-}42}$-induced inflammation in rat hippocampus *in vivo* and *in vitro* via inhibition of microglial activation and expression of pro-inflammatory cytokines, such as IL-1β (26). We recently demonstrated that in traumatic spinal cord injury, endogenous IL-4 neutralization profoundly increases the extent of ED-1-positive macrophage activation, resulting in more extensive cavitation (23). Furthermore, endogenous IL-13 and IL-4 control brain inflammation by reducing the levels of iNOS and TNF-α in LPS-treated rat cerebral cortices *in vivo*, resulting in enhanced neuronal survival (36, 40). These results collectively support the beneficial effects of IL-13 or IL-14 as anti-inflammatory cytokines.

Conversely, harmful effects of IL-13 or IL-4 have also been reported. For instance, an earlier study showed that IL-13 knockout mice display decreased numbers of infiltrating cells ($CD11b^+$) and MHC-II expression in experimental autoimmune encephalomyelitis (EAE), resulting in reduced EAE incidence (41). An exogenous IL-4 antibody has been shown to inhibit EAE progression via reduction of MCP-1 and RANTES levels (Regulated upon Activation, Normal T-cell Expressed, and Secreted; CCL5) in mice models (16). In a mouse model for allergic asthma, allergic airway inflammation was attenuated via inhibition of eosinophil recruitment in IL-4-deficient mice (5). Further studies on a mouse asthma model disclosed that an anti-IL-13 monoclonal antibody (inhibiting IL-13) prevents progression of inflammation by inhibiting the expression of cytokines and chemokines, such as TNF-α and MIP-1α (53, 54). IL-13 and IL-4 antagonists (Pitrakinra) have been used as therapeutic drugs in human asthma (14, 49). These cytokines also induce NADPH oxidase activation and consequent production of ROS in endothelial cells (18, 47). We recently showed that IL-13 or IL-4 induces activation of NADPH oxidase and/or iNOS and consequent ROS production in a thrombin-treated CA1 layer of hippocampus *in vivo* (33, 34), leading to oxidative damage and eventual neurodegeneration. Clearly, IL-13 and IL-4 contribute to neurotoxicity by stimulating NADPH oxidase and/or iNOS activity for ROS production. This hypothesis is strongly supported by our current data showing that neutralization of IL-13 or IL-4 inhibits ROS generation in A$\beta_{1\text{-}42}$-treated hippocampus via attenuation of oxidative damage caused by microglia-derived NADPH oxidase and/or iNOS, eventually promoting neuronal survival.

As discussed recently, the current results are not consistent with our previous report showing that IL-13 or IL-4 controls brain inflammation, resulting in the reduction of iNOS and TNF-α expression and eventual enhancement of neuronal survival in LPS-injected cortex *in vivo* (36, 40). In the present study, we demonstrated that both IL-13 and IL-4 mediate the production of iNOS and NADPH oxidase-derived ROS, leading to neurodegeneration in the A$\beta_{1\text{-}42}$-injected CA1 layer of hippocampus *in vivo*. This finding is in keeping with our recent data showing that IL-13 or IL-4 contribute to the production of pro-inflammatory cytokines (TNF-α and IL-1β), and iNOS and NADPH oxidase-derived ROS, leading to neurodegeneration in the thrombin-treated CA1 layer of hippocampus *in vivo* (33, 34). These apparent discrepancies may be attributed to the use of different stimuli (LPS *vs* A$\beta_{1\text{-}42}$ or thrombin) and/or target areas (cortex *vs.* hippocampus), although the underlying mechanisms remain to be determined. This interpretation is further supported by our unpublished observation that IL-13 and/or IL-4 expression within activated microglia is evident in both A$\beta_{1\text{-}42}$ and thrombin-treated cortices and LPS-treated hippocampus in a time-dependent manner (data not shown).

To our knowledge, this is the first study to demonstrate the possible involvement of endogenously expressed IL-13 and/or IL-4 in activated microglia after A$\beta_{1\text{-}42}$ injection in the degeneration of hippocampal neurons. Recently, we showed that IL-13 and IL-4 induce activation of microglial NADPH oxidase, thereby enhancing ROS and iNOS production in the CA1 layer of hippocampus treated with thrombin (33, 34). Similar to A$\beta_{1\text{-}42}$, thrombin may be one of the main factors causing AD, since it is neurotoxic to hippocampal neurons both *in vivo* and *in vitro* (33, 34), and its immunoreactivity is increased, whereas that of the thrombin inhibitor protease, nexin I, is significantly reduced in the brain of AD patients (2, 10, 46). Moreover, thrombin modulates the production of amyloid protein precursors and their cleavage into fragments detected in amyloid plaques of AD brains (12, 20). The current findings, in combination with data on thrombin, suggest that the deleterious effects of microglia-derived endogenous IL-13 and/or IL-4 are involved in oxidative stress-mediated neurodegenerative diseases, such as AD.

Finally, oxidative stress was shown to activate cellular stress-responsive and antioxidative genes called vitagenes, including heme oxygenase-1 (HO-1) (7). HO-1 was significantly increased in endothelial cells exposed to oxidative stress such as endotoxins and cytokines and in AD brain (7). The beneficial effects of HO-1 in AD raise possibilities that HO-1 is a promising drug for the prevention and treatment of AD. Regarding this, Liu and colleagues (24) demonstrated that IL-13 reduced HO-1 expression in LPS-activated rat microglia, resulting in aggravation of activated microglia death. IL-13 and IL-4 also downregulated expression of HO-1 mRNA and protein in cultured normal human epidermal keratinocytes (31). Therefore, it is likely that endogenously expressed IL-13 and IL-4 might serve as neurotoxic mediators by downregulating AD-related vitagenes such as HO-1 in A$\beta_{1\text{-}42}$-treated hippocampus *in vivo*.

Materials and Methods

Preparation of Aβ peptide

Full length of A$\beta_{1\text{-}42}$ or reverse peptide A$\beta_{42\text{-}1}$ (Invitrogen, Camarillo, CA) were prepared as described previously (38) by dissolving the peptide in a freshly prepared 35% acetonitrile solution with dilution to a final concentration of 500 μM in 0.1 *M* phosphate buffer saline (PBS, pH 7.4). The A$\beta_{1\text{-}42}$ or A$\beta_{42\text{-}1}$ solution was incubated for 18 h at 37°C to prepare fibrillar aggregates. After incubation, A$\beta_{1\text{-}42}$ or A$\beta_{42\text{-}1}$ solutions were stored at −20°C until use.

Stereotaxic surgery and drug injection

All surgical experiments were performed in accordance with Guidelines and Polices for Rodent Survival Surgery provided by the Animal Care Committee of the Kyung Hee University. Female Sprague Dawley (SD) rats (11 weeks, 230–250 g) were anesthetized by injection of chloral hydrate (Sigma, St. Louis, MO, 360 mg/kg, i.p.) and positioned in a stereotaxic apparatus (David Kopf Instruments, Tujunga,

CA). A midline sagittal incision was made in the scalp, and holes were drilled in the skull over dorsal hippocampus using the following coordinates: 3.6 mm posterior to bregma and 2.0 mm lateral to the midline for intrahippocampal injections according to the atlas of Paxinos and Watson (37). The hole of the tip was directed down to 2.6 mm beneath the surface of the brain for the hippocampus. All injections were made using a Hamilton syringe equipped with a 30S gauge beveled needle and attached to a syringe pump (KD Scientific, New Hope, PA). Infusions were made at a rate of 0.2 μl/min for A$\beta_{1\text{-}42}$ (1 nmol in 2 μl). As described in our previous reports (23, 33, 34, 36, 40), for neutralization, some animals received either 1 nmol of A$\beta_{1\text{-}42}$ or co-injection of A$\beta_{1\text{-}42}$ and anti-murine IL-13 neutralizing antibody/IL-4 neutralizing antibody, or nonspecific murine IgG as a control (1 μg; R&D Systems, Minneapolis, MN). As described, trolox (50 mg/kg, i.p; Sigma) (11, 52) or NAC (150 mg/kg, i.p) (3, 35) was injected 30 min before A$\beta_{1\text{-}42}$ treatment. After injection, the needle was left in place for an additional 5 min before being slowly retracted. Intact (noninjected) or A$\beta_{42\text{-}1}$-injected animals were used as controls.

Transgenic mice and genotyping

A pathogen-free transgenic line of Alzheimer's disease mouse model, APP/PS1 mice (21), was obtained from Jackson Laboratory (Bar Harbor, ME) and maintained by crossing transgenic males with B6C3F1 females that were purchased from Jackson Lab. APP/PS1 mice carry mouse APP with the double mutations (K670N and M671L) and human PS1 with a deletion of exon 9 found in familial AD patients. The genotyping for the APP/PS1 transgene was performed by the PCR-based method provided by the Jackson Lab. APP/PS1 mice used were 8–12 months old. For each experimental group, 4–5 mice were used. For PCR analysis, genomic DNA was prepared from tails of adult mice, and specific primers were used. The following primer pairs were used: APP forward 5′-GAC TGA CCA CTC GAC CAG GTT CTG-3′; APP reverse 5′-CTT GTA AGT TGG ATT CTC ATA TCC G-3′; PS1 forward 5′-AAT AGA GAA CGG CAG GAG CA-3′; PS1 reverse 5′-GCC ATG AGG GCA CTA ATC AT-3′.

Tissue preparation and immunohistochemistry

Animals were anesthetized with chloral hydrate (360 mg/kg, i.p.) at the indicated time points after injection and transcardially perfused with saline solution containing 0.5% sodium nitrate and heparin (10 U/ml), followed by fixation with 4% paraformaldehyde dissolved in 0.1 *M* phosphate buffer (PB). Brains were removed from the skull, post-fixed overnight at 4°C in buffered 4% paraformaldehyde, and stored at 4°C in 30% sucrose solution until they sank. Brains were frozen sectioned using a sliding microtome into 40 μm coronal sections and collected in six separate series. Immunohistochemistry was performed using the avidin-biotin staining technique as described previously (11). Briefly, free-floating serial sections were rinsed three times for 10 min in PBS and then pretreated for 5 min at room temperature in PBS containing 1% H_2O_2. Sections were then rinsed in PBS containing 0.3% Triton X-100 and 0.5% BSA and then pre-incubated for 1 h at room temperature in PBS containing 0.5% BSA. Next, the sections were incubated overnight with gentle shaking at room temperature with PBS containing 0.5% BSA and the following monoclonal primary antibodies: OX-42 (CD11b, 1:200; Serotec, Oxford, UK), which recognizes complement receptor 3; OX-6 (CD74, 1:200; Serotec), which recognizes major histocompatibiltiy complex II antigens and stains microglia; 8-hydroxy-2′-deoxyguanosin (8-OHdG; 1:200; JalCA, Shizuoka, Japan), which is a marker of oxidative stress to DNA, and the neuronal-specific nuclear protein NeuN (1:400; Chemicon, Temecula, CA) as a general stain for neurons. Sections were then rinsed in PBS and incubated for 1 h at room temperature in biotin-conjugated anti-mouse antibody (KPL, Gaithersburg, MD) in PBS containing 0.5% BSA. Sections were rinsed again and incubated for 1 h at room temperature in avidin-biotin complex solution (Vector Laboratories, Burlingame, CA). After rinsing three times in PBS, the signal was detected by incubating sections in 0.5 mg/ml 3,3′-diaminobenzidine (Sigma) in 0.1 *M* PB containing 0.003% H_2O_2. Sections were then rinsed in PBS, mounted on gelatin-coated slides, and viewed under a bright-field microscope (Olympus Optical, Tokyo, Japan). For Nissl staining, some of the hippocampus tissue was mounted on gelatin-coated slides, dried for 1 h at room temperature, stained with 0.5% cresyl violet (Sigma), dehydrated, coverslipped, and then analyzed under a bright-field microscope (Olympus Optical, Tokyo, Japan).

Double-immunofluorescence staining

For immunofluorescence staining, sections were processed as described previously (11). Briefly, sections were mounted on gelatin-coated slides, dried for 1 h at room temperature, and washed twice in PBS. Slides were incubated for 30 min in PBS containing 0.2% Triton X-100. After blocking with 0.5% BSA, slides were incubated overnight at 4°C with OX-42, MAC-1 (1:200, Serotec), and following combination: OX-42 or MAC-1 and goat anti-IL-13/ IL-4 antibody (1: 2000, R&D Systems, Minneapolis, MN) or $p67^{phox}$/$p47^{phox}$ (1:200; Santa Cruz Biotechnology, Santa Cruz, CA). After thorough rinsing in PBS, slides were covered for 1 h at room temperature with a mixture of Texas Red-conjugated anti-goat IgG, fluorescein-conjugated anti-mouse IgG, fluorescein-conjugated *Lycopersicon esculentum* (tomato) lectin (1:200; Vector Laboratories, Burlingame, CA) and Alexa Flour® 594 anti-rabbit (1:200; Molecular Probes, Eugene, OR). Slides were then rinsed three times with PBS, coverslipped with Vectashield medium (Vector Laboratories), and analyzed using IX71 confocal microscope (Olympus Optical).

In situ *detection of superoxide and* $O_2^{\bullet-}$*-derived oxidants*

Hydroethidine histochemistry was performed for *in situ* visualization of $O_2^{\bullet-}$ and $O_2^{\bullet-}$ derived oxidants (11). Five days after injection, hydroethidine (1 mg/ml in PBS containing 1% dimethylsulfoxide; Molecular Probes) was administered intraperitoneally. After 15 min, the animals were transcardially perfused with a saline solution containing 0.5% sodium nitrate and heparin (10 U/ml) and then fixed with 4% paraformaldehyde in 0.1 *M* PB. After fixation, the brains were cut into 40 μm slices using a sliding microtome. Sections were mounted on gelatin-coated slides, and the oxidized hydroethidine product, ethidium, was examined by IX71 confocal microscopy (Olympus Optical).

Western blot analysis

Brain tissues from the ipsilateral hippocampus were dissected and homogenized in ice-cold lysis buffer containing the

following (in m*M*): 20 Tris-HCl (pH 7.5), 1 EDTA, 5 $MgCl_2$, 1 dithiothreitol, 0.1 phenylmethylsulfonyl fluoride, and protease inhibitor mixture (Roche, Mannheim, Germany). The tissue homogenates was centrifuged at 4°C for 20 min at 14,000 *g*, and the supernatant was transferred to a fresh tube. The extracts were frozen and kept at −80°C. For subcellular fractionation, protein extracts of both the cytosolic and plasma membrane factions were prepared from the ipsilateral hippocampus at the indicated time points after injection. Tissues were gently homogenized using a glass homogenizer in ice-cold buffer consisting of the following (in m*M*): 20 HEPES, 250 sucrose, 10 KCl, 1.5 $MgCl_2$, 2 EDTA, and protease inhibitor mixture. Homogenates were centrifuged for 5 min at 500 *g* at 4°C, and supernatants were collected and centrifuged for 20 min at 13,000 *g* at 4°C. The pellets were further centrifuged for 1 h at 100,000 *g* at 4°C, and the resulting supernatants and pellets were designated as the cytosolic and plasma membrane fractions, respectively. Equal amounts of protein (50 μg) were mixed with loading buffer (0.125 m*M* Tris-HCl, pH 6.8, 20% glycerol, 4% SDS, 10% mercaptoethanol, and 0.002% bromophenol blue), boiled for 5 min, and separated by SDS-PAGE. After electrophoresis, proteins were transferred to polyvinylidene difluoride membranes (PVDF, Millipore, Temecula, CA) using an electrophoretic transfer system (Bio-Rad, Hercules, CA). The membranes were washed with Tris-buffered saline solution (TBS) and then blocked for 1 h in TBS containing 5% skim milk. The membranes were then incubated overnight at 4°C with one of the following the specific primary antibodies: rabbit anti-iNOS (1:1000; Upstate Biotechnology, Lake Placid, NY), mouse anti-$p67^{phox}$ (1:500; BD Biosciences, Franklin Lakes, NJ), rabbit anti-$p47^{phox}$ (1:200; Santa Cruz Biotechnology), mouse anti-IL-13 (1:200; R&D System, Minneapolis, MN), goat anti-IL-4 (1:300 Santa Cruz Biotechnology), and 4-hydroxy-2-nonenal (HNE; 1:1000; alpha diagnostic, San Antonio, TX). After washing, the membranes were incubated for 1 h at room temperature with secondary antibodies (1:2000; Amersham Biosciences, Buckinghamshire, UK) and washed again. Finally, the blots were developed with enhanced chemiluminescence detection reagents (Amersham Biosciences). The blots were reprobed with antibodies against β-actin (1:4000; Santa Cruz Biotechnology) and α-atinin (1:2000 Santa Cruz Biotechnology). To determine the relative degree of membrane purification, the membrane fraction was subjected to immunoblotting for calnexin, a membrane marker, using a rabbit polyclonal antibody against calnexin (1:4000; Santa Cruz Biotechnology). For semiquantitative analyses, the densities of bands on immunoblots were measured with the Computer Imaging Device and accompanying software (Fujifilm).

Detection of protein oxidation and lipid peroxidation

The extent of protein oxidation lipid peroxidation was assessed by measuring protein carbonyl and lipid peroxidation levels with an OxyBlot protein oxidation detection kit (Chemicon, Billerica, MA) and OxiSelect™ Malondialdehyde (MDA) immune kit (Cell Biolabs, San Diego, CA) according to the protocol of the manufacturer as described previously (13, 33, 34). Protein samples were prepared from rat brains harvested 5 days after injection. Subsequently, for protein oxidation samples (15 μg) were mixed in a microcentrifuge tube with 5 μl of 12% SDS and 10 μl of 1x 2,4-dinitrophenylhydrazine (DNPH) solution. Ten microliters of 1x neutralization solution (a kit component) was added instead of the DNPH solution as the negative control. Tubes were incubated at room temperature for 15 min and then mixed with 7.5 μl of neutralization solution. Next, the samples were mixed in equal volumes of SDS sample buffer and separated by SDS-PAGE. After electrophoresis, proteins were transferred to polyvinylidene difluoride membranes. The membranes were then blocked for 1 h at room temperature in TBS containing 0.1% Tween-20 and 1% BSA. Membranes were incubated overnight at room temperature with the anti-DNPH antibody (1:150, a kit component) and then incubated at room temperature for 1 h with secondary antibodies (1:300, a kit component). Blots were developed using enhanced chemiluminescence reagents. Proteins that underwent oxidative modification (*i.e.,* carbonyl group formation) were identified as a band in the samples derivative with DNPH. For peroxidation protein sample (15 μg), tissue were washed with ice-cold PBS and homogenized with RIPA lysis buffer contains the fallowing (in m*M*); 150 NaCl, 10 Na_2PO_4 (pH 7.2), 0.5% sodium deoxycholate, 1% NP-40, and protease inhibitor mixture-free EDTA. The samples were incubated in a 4°C cold chamber. Next, samples were centrifuged at 4°C for 20 min 15,000 rpm. Supernatants were transferred to a fresh tube. The sample were mixed with loading buffer and boiled for 7 min, and separated by SDS-PAGE. The next step was the same as protein oxidation, but membranes were incubated overnight with rabbit anti-malondialdehyde (1:1000, a kit component) in a 4°C cold chamber. After washing, the membranes were incubated goat anti-rabbit HRP peroxidadase (1:1000, a kit component) for 1 hour. Blots were developed using enhanced chemiluminescence reagents. The optical density of the bands was measured using the Computer Imaging Device and accompanying software (Fujifilm). Levels of protein carbonyls were quantified and expressed as the fold increase versus untreated controls.

IL-13/4 sandwich ELISA

The production of IL-13/4 from rat hippocampus was determined by sandwich enzyme-linked immunosorbent assay (ELISA) techniques. Rat hippocampus tissue homogenized by tissue lysis buffer (a kit components) (33, 34). The samples were incubated in a 4°C cold chamber for overnight. Next, the sample centrifuged 14,000 *g* at 4°C for 20 min. Equal amounts of protein (100 μg) from each sample were placed in a ELISA kit strip coated with appropriates Ab. Sandwich ELISA was then performed according to the manufacturer's instructions. (Ray Biotech, Norcross, GA).

8-OHdG ELISA measurement

The production of DNA oxidation from rat hippocampus was determined by the 8-OHdG sandwich ELISA technique. Genomic DNA from rat hippocampal CA1 layer was extracted according the manufacturer's instructions (Wako, Osaka, Japan) and hydrolyzed by Nuclease P_1 and alkaline phosphatase buffer (a kit component). 8-OHdG levels were measured using sandwich ELISA technique according to the highly sensitive 8-OHdG Check instructions (Wako).

Counting of hippocampal CA1 neurons

The number of CA1 neurons was assessed at three levels of the dorsal hippocampus. Specifically, alternate sections were

obtained at 3.3, 3.6, 4.16, and 4.3 mm posterior to the bregma, and two regions from each level ($n = 8$ regions for each animal) were used to count cells in the CA1 region. The number of neurons within the CA1 layer was counted using a light microscope (Olympus Optical) at a magnification of 400X and expressed as the number of CA1 neurons per millimeter of linear length, as described previously (11). To maintain consistency across animals, a rectangular box (0.5×0.05 mm) was centered over the CA1 cell layer beginning 1.5 mm lateral to the midline. Only neurons with normal visible nuclei were counted. The mean number of CA1 neurons per millimeter for both hemispheres was calculated for each treatment group.

Statistical analysis

All values are expressed as mean ± SEM. Statistical significance ($p < 0.05$ for all analyses) was assessed by ANOVA using Instat 3.05 (GraphPad Software, San Diego, CA), followed by Student-Newman-Keuls analyses.

Acknowledgments

This research was supported by Basic Science Research Program through the National Research Foundation of Korea (NRF) funded by the Ministry of Education, Science and Technology (20090063274)

Author Disclosure Statement

No competing financial interests exist.

References

1. Akiyama H, Barger S, Barnum S, Bradt B, Bauer J, Cole GM, Cooper NR, Eikelenboom P, Emmerling M, Fiebich BL, Finch CE, Frautschy S, Griffin WS, Hampel H, Hull M, Landreth G, Lue L, Mrak R, Mackenzie IR, Mcgeer PL, O'banion MK, Pachter J, Pasinetti G, Plata-Salaman C, Rogers J, Rydel R, Shen Y, Streit W, Strohmeyer R, Tooyoma I, Van Muiswinkel FL, Veerhuis R, Walker D, Webster S, Wegrzyniak B, Wenk G, and Wyss-Coray T. Inflammation and Alzheimer's disease. *Neurobiol Aging* 21: 383–421, 2000.
2. Akiyama H, Ikeda K, Kondo H, and Mcgeer PL. Thrombin accumulation in brains of patients with Alzheimer's disease. *Neurosci Lett* 146: 152–154, 1992.
3. Bergamini S, Rota C, Canali R, Staffieri M, Daneri F, Bini A, Giovannini F, Tomasi A, and Iannone A. N-acetylcysteine inhibits *in vivo* nitric oxide production by inducible nitric oxide synthase. *Nitric Oxide* 5: 349–360, 2001.
4. Block ML. NADPH oxidase as a therapeutic target in Alzheimer's disease. *BMC Neurosci* 9: S8, 2008.
5. Brusselle GG, Kips JC, Tavernier JH, Van Der Heyden JG, Cuvelier CA, Pauwels RA, and Bluethmann H. Attenuation of allergic airway inflammation in IL-4 deficient mice. *Clin Exp Allergy* 24: 73–80, 1994.
6. Butovsky O, Talpalar AE, Ben-Yaakov K, and Schwartz M. Activation of microglia by aggregated beta-amyloid or lipopolysaccharide impairs MHC-II expression and renders them cytotoxic whereas IFN-gamma and IL-4 render them protective. *Mol Cell Neurosci* 29: 381–393, 2005.
7. Calabrese V, Cornelius C, Mancuso C, Pennisi G, Calafato S, Bellia F, Bates TE, Giuffrida Stella AM, Schapira T, Dinkova Kostova AT, and Rizzarelli E. Cellular stress response: A novel target for chemoprevention and nutritional neuroprotection in aging, neurodegenerative disorders and longevity. *Neurochem Res* 33: 2444–2471, 2008.
8. Cash E, Minty A, Ferrara P, Caput D, Fradelizi D, and Rott O. Macrophage-inactivating IL-13 suppresses experimental autoimmune encephalomyelitis in rats. *J Immunol* 153: 4258–4267, 1994.
9. Chao CC, Molitor TW, and Hu S. Neuroprotective role of IL-4 against activated microglia. *J Immunol* 151: 1473–1481, 1993.
10. Choi BH, Kim RC, Vaughan PJ, Lau A, Van Nostrand WE, Cotman CW, and Cunningham DD. Decreases in protease nexins in Alzheimer's disease brain. *Neurobiol Aging* 16: 557–562, 1995.
11. Choi SH, Lee DY, Kim SU, and Jin BK. Thrombin-induced oxidative stress contributes to the death of hippocampal neurons *in vivo*: Role of microglial NADPH oxidase. *J Neurosci* 25: 4082–4090, 2005.
12. Chong YH, Jung JM, Choi W, Park CW, Choi KS, and Suh YH. Bacterial expression, purification of full length and carboxyl terminal fragment of Alzheimer amyloid precursor protein and their proteolytic processing by thrombin. *Life Sci* 54: 1259–1268, 1994.
13. Chung YC, Kim SR, and Jin BK. Paroxetine prevents loss of nigrostriatal dopaminergic neurons by inhibiting brain inflammation and oxidative stress in an experimental model of Parkinson's disease. *J Immunol* 185: 1230–1237, 2010.
14. Corren J. Cytokine inhibition in severe asthma: Current knowledge and future directions. *Curr Opin Pulm Med* 17: 29–33, 2011.
15. Cross AR and Segal AW. The NADPH oxidase of professional phagocytes—Prototype of the NOX electron transport chain systems. *Biochim Biophys Acta* 1657: 1–22, 2004.
16. Furlan R, Poliani PL, Marconi PC, Bergami A, Ruffini F, Adorini L, Glorioso JC, Comi G, and Martino G. Central nervous system gene therapy with interleukin-4 inhibits progression of ongoing relapsing-remitting autoimmune encephalomyelitis in Biozzi AB/H mice. *Gene Ther* 8: 13–19, 2001.
17. Gordon MN, Holcomb LA, Jantzen PT, Dicarlo G, Wilcock D, Boyett KW, Connor K, Melachrino J, O'callaghan JP, and Morgan D. Time course of the development of Alzheimer-like pathology in the doubly transgenic PS1+ APP mouse. *Exp Neurol* 173: 183–195, 2002.
18. Harper RW, Xu C, Eiserich JP, Chen Y, Kao CY, Thai P, Setiadi H, and Wu R. Differential regulation of dual NADPH oxidases/peroxidases, Duox1 and Duox2, by Th1 and Th2 cytokines in respiratory tract epithelium. *FEBS Lett* 579: 4911–4917, 2005.
19. Hensley K, Maidt ML, Yu Z, Sang H, Markesbery WR, and Floyd RA. Electrochemical analysis of protein nitrotyrosine and dityrosine in the Alzheimer brain indicates region-specific accumulation. *J Neurosci* 18: 8126–8132, 1998.
20. Igarashi K, Murai H, and Asaka J. Proteolytic processing of amyloid beta protein precursor (APP) by thrombin. *Biochem Biophys Res Commun* 185: 1000–1004, 1992.
21. Jankowsky JL, Slunt HH, Gonzales V, Jenkins NA, Copeland NG, and Borchelt DR. APP processing and amyloid deposition in mice haplo-insufficient for presenilin 1. *Neurobiol Aging* 25: 885–892, 2004.
22. Janus C and Westaway D. Transgenic mouse models of Alzheimer's disease. *Physiol Behav* 73: 873–886, 2001.
23. Lee SI, Jeong SR, Kang YM, Han DH, Jin BK, Namgung U, and Kim BG. Endogenous expression of interleukin-4 regulates macrophage activation and confines cavity formation

after traumatic spinal cord injury. *J Neurosci Res* 88: 2409–2419, 2010.
24. Liu SH, Yang CN, Pan HC, Sung YJ, Liao KK, Chen WB, Lin WZ, and Sheu ML. IL-13 downregulates PPAR-gamma/heme oxygenase-1 via ER stress-stimulated calpain activation: aggravation of activated microglia death. *Cell Mol Life Sci* 67: 1465–1476, 2010.
25. Lovell MA and Markesbery WR. Ratio of 8-hydroxyguanine in intact DNA to free 8-hydroxyguanine is increased in Alzheimer disease ventricular cerebrospinal fluid. *Arch Neurol* 58: 392–396, 2001.
26. Lyons A, Griffin RJ, Costelloe CE, Clarke RM, and Lynch MA. IL-4 attenuates the neuroinflammation induced by amyloid-beta *in vivo* and *in vitro. J Neurochem* 101: 771–781, 2007.
27. Matsukawa A, Hogaboam CM, Lukacs NW, Lincoln PM, Evanoff HL, Strieter RM, and Kunkel SL. Expression and contribution of endogenous IL-13 in an experimental model of sepsis. *J Immunol* 164: 2738–2744, 2000.
28. Medeiros R, Prediger RD, Passos GF, Pandolfo P, Duarte FS, Franco JL, Dafre AL, Di Giunta G, Figueiredo CP, Takahashi RN, Campos MM, and Calixto JB. Connecting TNF-alpha signaling pathways to iNOS expression in a mouse model of Alzheimer's disease: Relevance for the behavioral and synaptic deficits induced by amyloid beta protein. *J Neurosci* 27: 5394–5404, 2007.
29. Millucci L, Ghezzi L, Bernardini G, and Santucci A. Conformations and biological activities of amyloid beta peptide 25–35. *Curr Protein Pept Sci* 11: 54-6-7, 2010.
30. Moon JH, Kim SY, Lee HG, Kim SU, and Lee YB. Activation of nicotinic acetylcholine receptor prevents the production of reactive oxygen species in fibrillar beta amyloid peptide (1-42)-stimulated microglia. *Exp Mol Med* 40: 11–18, 2008.
31. Numata I, Okuyama R, Memezawa A, Ito Y, Takeda K, Furuyama K, Shibahara S, and Aiba S. Functional expression of heme oxygenase-1 in human differentiated epidermis and its regulation by cytokines. *J Invest Dermatol* 129: 2594–2603, 2009.
32. Paludan SR, Lovmand J, Ellermann-Eriksen S, and Mogensen SC. Effect of IL-4 and IL-13 on IFN-gamma-induced production of nitric oxide in mouse macrophages infected with herpes simplex virus type 2. *FEBS Lett* 414: 61–64, 1997.
33. Park KW, Baik HH, and Jin BK. Interleukin-4-induced oxidative stress via microglial NADPH oxidase contributes to the death of hippocampal neurons *in vivo. Curr Aging Sci* 1: 192–201, 2008.
34. Park KW, Baik HH, and Jin BK. IL-13-induced oxidative stress via microglial NADPH oxidase contributes to death of hippocampal neurons *in vivo. J Immunol* 183: 4666–4674, 2009.
35. Park KW and Jin BK. Thrombin-induced oxidative stress contributes to the death of hippocampal neurons: Role of neuronal NADPH oxidase. *J Neurosci Res* 86: 1053–1063, 2008.
36. Park KW, Lee DY, Joe EH, Kim SU, and Jin BK. Neuroprotective role of microglia expressing interleukin-4. *J Neurosci Res.* 81: 397–402, 2005.
37. Paxinos G and Watson C. *The Rat Brain in Sterotaxic Coordinates.* San Diego: *Academic.* 1998.
38. Ryu JK, Franciosi S, Sattayaprasert P, Kim SU, and Mclarnon JG. Minocycline inhibits neuronal death and glial activation induced by beta-amyloid peptide in rat hippocampus. *Glia* 48: 85–90, 2004.
39. Shimohama S, Tanino H, Kawakami N, Okamura N, Kodama H, Yamaguchi T, Hayakawa T, Nunomura A, Chiba S, Perry G, Smith MA, and Fujimoto S. Activation of NADPH oxidase in Alzheimer's disease brains. *Biochem Biophys Res Commun* 273: 5–9, 2000.
40. Shin WH, Lee DY, Park KW, Kim SU, Yang MS, Joe EH, and Jin BK. Microglia expressing interleukin-13 undergo cell death and contribute to neuronal survival *in vivo. Glia* 46: 142–152, 2004.
41. Sinha S, Kaler LJ, Proctor TM, Teuscher C, Vandenbark AA, and Offner H. IL-13-mediated gender difference in susceptibility to autoimmune encephalomyelitis. *J Immunol* 180: 2679–2685, 2008.
42. Szaingurten-Solodkin I, Hadad N, and Levy R. Regulatory role of cytosolic phospholipase A2alpha in NADPH oxidase activity and in inducible nitric oxide synthase induction by aggregated Abeta1-42 in microglia. *Glia* 57: 1727–1740, 2009.
43. Szczepanik AM, Funes S, Petko W, and Ringheim GE. IL-4, IL-10 and IL-13 modulate A beta(1–42)-induced cytokine and chemokine production in primary murine microglia and a human monocyte cell line. *J Neuroimmunol* 113: 49–62, 2001.
44. Thinakaran G and Koo EH. Amyloid precursor protein trafficking, processing, and function. *J Biol Chem* 283: 29615–29619, 2008.
45. Tomlinson KL, Davies GC, Sutton DJ, and Palframan RT. Neutralisation of interleukin-13 in mice prevents airway pathology caused by chronic exposure to house dust mite. *PLoS One* 5: e13136, 2010.
46. Vaughan PJ, Su J, Cotman CW, and Cunningham DD. Protease nexin-1, a potent thrombin inhibitor, is reduced around cerebral blood vessels in Alzheimer's disease. *Brain Res* 668: 160–170, 1994.
47. Walch L, Massade L, Dufilho M, Brunet A, and Rendu F. Pro-atherogenic effect of interleukin-4 in endothelial cells: Modulation of oxidative stress, nitric oxide and monocyte chemoattractant protein-1 expression. *Atherosclerosis* 187: 285–291, 2006.
48. Weiner HL and Frenkel D. Immunology and immunotherapy of Alzheimer's disease. *Nat Rev Immunol* 6: 404–416, 2006.
49. Wenzel S, Wilbraham D, Fuller R, Getz EB, and Longphre M. Effect of an interleukin-4 variant on late phase asthmatic response to allergen challenge in asthmatic patients: Results of two phase 2a studies. *Lancet* 370: 1422–1431, 2007.
50. Wilkinson BL and Landreth GE. The microglial NADPH oxidase complex as a source of oxidative stress in Alzheimer's disease. *J Neuroinflamm* 3: 30, 2006.
51. Williamson KS, Gabbita SP, Mou S, West M, Pye QN, Markesbery WR, Cooney RV, Grammas P, Reimann-Philipp U, Floyd RA, and Hensley K. The nitration product 5-nitro-gamma-tocopherol is increased in the Alzheimer brain. *Nitric Oxide* 6: 221–227, 2002.
52. Won SY, Choi SH, and Jin BK. Prothrombin kringle-2-induced oxidative stress contributes to the death of cortical neurons *in vivo* and *in vitro*: role of microglial NADPH oxidase. *J Neuroimmunol* 214: 83–92, 2009.
53. Yang G, Li L, Volk A, Emmell E, Petley T, Giles-Komar J, Rafferty P, Lakshminarayanan M, Griswold DE, Bugelski PJ, and Das AM. Therapeutic dosing with anti-interleukin-13 monoclonal antibody inhibits asthma progression in mice. *J Pharmacol Exp Ther* 313: 8–15, 2005.
54. Yang G, Volk A, Petley T, Emmell E, Giles-Komar J, Shang X, Li J, Das AM, Shealy D, Griswold DE, and Li L. Anti-IL-13 monoclonal antibody inhibits airway hyperresponsiveness, inflammation and airway remodeling. *Cytokine* 28: 224–232, 2004.

55. Yu JT, Lee CH, Yoo KY, Choi JH, Li H, Park OK, Yan B, Hwang IK, Kwon YG, Kim YM, and Won MH. Maintenance of anti-inflammatory cytokines and reduction of glial activation in the ischemic hippocampal CA1 region preconditioned with lipopolysaccharide. *J Neurol Sci* 296: 69–78, 2010.

Address correspondence to:
Prof. Byung K. Jin
Department of Biochemistry and Molecular Biology
Neurodegeneration Control Research Center
School of Medicine, Kyung Hee University
Seoul 130-701
South Korea

E-mail: bkjin@khu.ac.kr

Date of first submission to ARS Central, July 19, 2011; date of final revised submission, January 11, 2012; date of acceptance, January 12, 2012.

Abbreviations Used

8-OHDG = 8-hydroxydeoxyguanosine
$A\beta_{1\text{-}42}$ = amyloid beta$_{1\text{-}42}$
$A\beta_{42\text{-}1}$ = amyloid beta$_{42\text{-}1}$
AD = Alzheimer's disease
CA1 = Cornu Ammonis 1
DAB = diaminobenzidine
GFAP = glial fibrillary acidic protein
HNE = 4-hydroxy-2-nonenal
HRP = horseradish peroxidase
IL-4 = interleukin-4
IL-4 NA = interlukin-13 neutralizing antibody
IL-13 = interlukin-13
IL-13 NA = interlukin-13 neutralizing antibody
IgG = immunoglobulin G
iNOS = inducible nitric oxide synthase
MAC-1 = macrophage-1
MDA = malondialdehyde
MS = multiple sclerosis
NAC = N-acetyl-L-cysteine
NADPH oxidase = nicotinamide adenine dinucleotide phosphate oxidase
NeuN = neuronal nuclei
OX-6(CD74) = cluster of differentiation molecule 74
OX-42(CD11b) = cluster of differentiation molecule 11B
Rac-1 = Ras-related C3 botulinum toxin substrate 1
ROS = reactive oxygen species